Nonlinear lattice-relaxation process of excitons in quasi-one-dimensional halogen-bridged mixed-valence metal complexes: Self-trapping, solitons, and polarons

Masato Suzuki and Keiichiro Nasu
Institute for Molecular Science, Graduate University for Advanced Studies, 38 Nishigo-naka, Myodaiji, Okazaki 444, Japan
(Received 28 January 1991; revised manuscript received 10 June 1991)

Self-trapped excitons, solitons, and polarons of a one-dimensional extended Peierls-Hubbard model are investigated, in order to clarify the lattice-relaxation paths of photogenerated excitons in halogen-bridged mixed-valence metal complexes. This theory takes into account the lattice distortion of halogen ions in a direction perpendicular to the chain, as well as in a parallel direction. It is mainly based on the adiabatic approximation for phonons and the mean-field theory for interelectronic interactions, but is also reinforced by taking into account the electron-hole correlation to obtain the exciton. Potential surfaces relevant to the relaxation of the exciton are clarified in terms of various nonlinear excitations. This result can explain rather diverse experiments from a unified point of view, such as photoabsorption and luminescence spectra, the Stark effect, and electron-spin-resonance data. The origin of the photoinduced absorption is concluded to be polarons.

I. INTRODUCTION

Theoretical[1,14–17] and experimental[2–13] problems related to the nonlinear lattice-relaxation process of an exciton in quasi-one-dimensional charge-density-wave (CDW) states have been subjects of considerable interest in recent years. The CDW is quite an exotic insulating state, because photogenerated excitons proliferate during lattice relaxation. The word "nonlinear" is introduced so as to emphasize this characteristic feature, as compared with the ordinary insulators. In this paper, we will be concerned with the nonlinear lattice relaxation of an exciton in halogen-bridged mixed-valence metal complexes (HMMC's), as typical examples for quasi-one-dimensional CDW states.

The HMMC is composed of transition-metal ions $M^{3+}(\equiv Pt^{3+}, Pd^{3+}, Ni^{3+})$ bridged by halogen ions $X^{-}(\equiv Cl^{-}, Br^{-}, I^{-})$, as schematically shown in Fig. 1. M^{3+} is coordinated by a ligand ($\equiv AA$), where AA is a planer organic molecule such as ethylenediamine (en), ethylamine (etn), or cyclohexanediamine. These AA's are bound together through the counterions ($\equiv Y$'s), where Y is ClO_4^- or BF_4^-. The Y's bring about a weak interchain interaction, and contribute to the stability of the HMMC chain. The essential factor that determines the electronic properties of the HMMC is the strong coupling between an unpaired electron in the d_{z^2} orbital of M^{3+} and the vibrational modes (or phonon) of the X^- (the z axis is parallel to the chain). This strong coupling brings about various nonlinear phenomena in the lattice-relaxation process of the exciton.

Let us briefly consider the photogeneration of an exciton and its associated relaxation processes. As is well known, the one-dimensional metallic state for the electrons is unstable against the strong electron-phonon (e-ph) interaction, and it results in the Peierls transition.[18] In case of HMMC, it has been confirmed by various experiments that the charge transfer occurs between two neighboring M's so as to give the following mixed-valence state:

$$\cdots X^- - M^{+(3+\delta)} - X^- \cdots M^{+(3-\delta)} \cdots X^- - M^{+(3+\delta)} - X^- \cdots$$
$$- X^- \cdots M^{+(3-\delta)} \cdots X^- - M^{+(3+\delta)} - X^- \cdots M^{+(3-\delta)} \cdots X^- -$$

where the X^-'s have been distorted with a periodicity which is twice the period of the original lattice. δ denotes the degree of charge transfer.

This is nothing but the CDW state, which is doubly degenerate according to the two possible phases of the Peierls distortion, as seen above. In this CDW state, the d_{z^2} electrons are influenced by the potential energy as schematically shown in Fig. 2(a). Because of the electrostatic repulsion of X^-, the d_{z^2} orbitals become alternately higher and lower as the X^- approaches or leaves the neighboring M^{3+}.

The HMMC has a strong light absorption band in the visible region, corresponding to the charge-transfer (CT) excitation of an electron from the occupied d_{z^2} orbital to vacant ones, as shown in Fig. 2(b). Thus an electron and a hole are created, and they attract each other through the interorbital Coulombic force. Such a state is usually called a CT exciton.

Because of this backward charge transfer, however, the electron number per orbital becomes almost equal in this region, and the Peierls distortion has lost the reason for its presence. Hence, it therefore tends to disappear, as

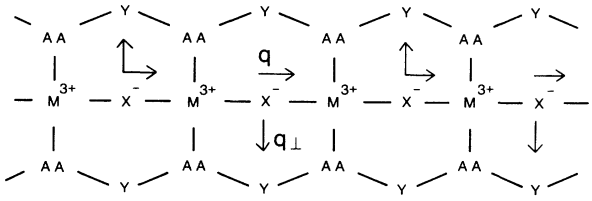

FIG. 1. Schematic structure of HMMC. $M^{3+}=Pt^{3+}$, Pd^{3+}, or Ni^{3+}. $X^{-}=Cl^{-}$, Br^{-}, or I^{-}. AA and Y denote a ligand and a counterion, respectively.

seen from Fig. 2(c). Thus the exciton self-induces a local lattice distortion, and is trapped in it. This is usually called a self-trapped exciton (STE).

Even in the case of ordinary insulators. The STE appears after the lattice relaxation, provided that the exciton couples strongly with the phonons. In that case, however, the STE is the end result of the lattice relaxation. In the case of the CDW considered here, the STE is not the lowest excited state, and will undergo further relaxations, which come from the twofold degeneracy of the ground state. In the CDW, as is well known, we have a low-lying excited state with a collective nature. That is, one phase of the ground state can appear locally in the other phase of the ground state at the expense of creating boundaries between the two phases. This boundary is usually called a soliton, and the exciton is expected to finally relax down to the state with a pair of solitons, as shown in Fig. 2(d). In contrast to the case of single charge transfer, a great number of charges have been transferred to cause this pair state to appear, and this is nothing but a nonlinear lattice relaxation of the exciton.

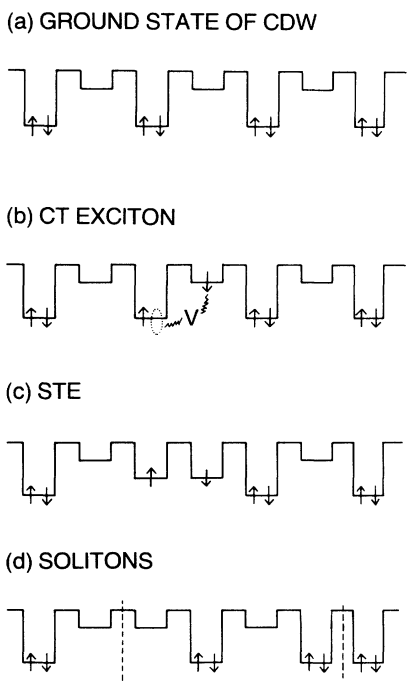

FIG. 2. Schematical potential energy for the d_{z^2} electrons: (a) the ground state of CDW, (b) the CT exciton, (c) the STE, (d) the solitons. Small arrows correspond to the electron with each spin.

Let us briefly survey the experimental studies for the relaxation process of the exciton in $[Pt(en)_2][Pt(en)_2Cl_2](ClO_4)_4$, which is typical HMMC. Hereafter, we will call it the "Pt-Cl complex."

Wada *et al.* have observed a strong light absorption band of the Pt-Cl complex in the visible region, which corresponds to the aforementioned CT exciton, and its peak energy is 2.7 eV.[2] Recently, Wada *et al.* also determined the binding energy of the exciton, using electric-field effects, and this energy turned out to be 20–30 % of the free-electron-hole pair excitation energy.[3] This result indicates that the strong electron-hole correlation must be accounted for in a theoretical description of this HMMC.

Luminescence spectra from the STE have been obtained by Tanino and Kobayashi[4] and Tanaka *et al.*[5] Their energy is 1.2 eV, being 45% of the exciton energy. Such a large Stokes shift indicates that the *e*-ph coupling is strong in this material. The luminescence lifetime has also been determined to be about 100 ps.[6,7] This is exceptionally short compared with the lifetime of STE's in ordinary insulators, such as alkali halides, for which it is about 10^{-8} s. This means that the STE is not the final state of lattice relaxation, but there are lower-lying excited states intrinsic to the CDW.

In connection with such low-lying excited states, Kurita and co-workers have recently found that two extra light absorption bands appear in the energy-gap region of the CDW, when the CT band is excited by an intense laser light.[8,9] These photoinduced absorption bands are called the A and B bands, and their respective peak energies are 70% and 80% of the exciton energy. More recently, two other bands C and D have been also found. C is 15% (Ref. 10) and D is more than 80% (Ref. 11) of the exciton energy. In addition to this photoinduced absorption. Kurita and co-workers found that the intensity of the electron spin resonance (ESR) signal increases as these bands develop. Thus the origin of these bands is concluded to have a spin.[9] From the analysis of its ESR signal, very recently, Kuroda *et al.* have proposed that the spin is localized only within two metallic sites.[12]

Our main purpose in the present paper is to clarify these eight rather diverse experiments from a unified theoretical point of view. In our previous theoretical works,[14–16] the exciton effect in the final state of the optical transition was not fully taken into account. Moreover, for the displacement of X^{-}, only the component longitudinal to the chain axis had been considered. Recently, however, Degiorigi *et al.*[13] have found from infrared measurements that the force constant of the X^{-} vibrations transverse to the chain axis is an order of magnitude smaller than the longitudinal ones. Furthermore, Yamashita and Toriumi[19] have recently synthesized a material that has a transverse displacement even in its ground state. Thus we are no longer justified in neglecting the transverse movements of X^{-} during the relaxation process.

Mishima and Nasu[14–16] have also studied this exciton problem theoretically. In their theory, however, the final state of the optical transition is not an exciton, but a free-electron-hole pair. For this reason, the exciton effect

has been left unsolved despite its importance.

Therefore, in this paper, we will introduce a model that takes into consideration both longitudinal and transverse movements of X^-, as well as excitonic effects. With this model, we will clarify the nonlinear lattice relaxation of the exciton.

II. SIX-PARAMETER MODEL

Let us now introduce a model Hamiltonian (H) to describe the nonlinear lattice-relaxation process of the exciton in the HMMC. H is given as ($\hbar=1$)

$$H=H_{\parallel}+H_{\perp} , \tag{1}$$

where

$$\begin{aligned} H_{\parallel}=&-T\sum_{l,\sigma}(a^{\dagger}_{l+1,\sigma}a_{l\sigma}+\text{H.c.})+\omega\sum_{l}q_l^2/2 \\ &+\sqrt{S\omega}\sum_{l,\sigma}(q_l-q_{l+1})n_{l\sigma}+U\sum_{l}n_{l\alpha}n_{l\beta} \\ &+V\sum_{l,\sigma,\sigma'}n_{l\sigma}n_{l+1,\sigma'} , \end{aligned} \tag{2}$$

and

$$\begin{aligned} H_{\perp}\equiv&-\sqrt{S_{\perp}\omega_{\perp}}\sum_{l,\sigma}|q_{\perp l}|(n_{l\sigma}+n_{l-1,\sigma}-1)+\omega_{\perp}\sum_{l}q_{\perp l}^2/2 \\ &-\sqrt{T'\omega_{\perp}}\sum_{l,\sigma}|q_{\perp l}|(a^{\dagger}_{l\sigma}a_{l-1,\sigma}+\text{H.c.}) \\ &+\sum_{l}F(q_{\perp l}q_{\perp,l-1}) . \end{aligned} \tag{3}$$

In these equations, $a^{\dagger}_{l\sigma}$ is the creation operator of the electron localized at metallic site l with spin σ ($=\alpha,\beta$), and T is the transfer energy between neighboring two d_{z^2} orbitals. q_l is the dimensionless coordinate of the longitudinal displacement of X^-, and ω is the energy of this phonon mode. Its kinetic energy is neglected under the adiabatic approximation. S is the site-diagonal e-ph coupling energy. U and V denote the intrasite and intersite Coulombic repulsive energies, respectively.

$H_{\perp}$ in Eq. (1) is associated with transverse movements. As we mentioned before, this part will become important even in the ground state in some HMMC's. Throughout this paper, however, we assume that it plays its role only after the exciton has separated into an electron and a hole, because it is only the electron that repels the X^-. $q_{\perp l}$ is the dimensionless coordinate of this displacement at the site l with the energy $\omega_{\perp}$. We consider the following two kinds of effects coming from this movement.

The first effect is the diagonal coupling between excess electrons and this transverse motion. When more than two electrons are on the two neighboring M's, the X^- between them will move away from the chain, so as to decrease the Coulombic repulsion. $S_{\perp}$ denotes the energy-lowering constant of this movement. Since this motion has even parity, the e-ph interaction should be proportional to $q_{\perp l}^2$ for very small displacements. However, when the displacement is large enough, it is expected to be proportional to $|q_{\perp l}|$. Since we only consider the equilibrium configuration with a relatively large displacement, we can assume this e-ph coupling to be proportional to $|q_{\perp l}|$.

The second effect of $H_{\perp}$ is an increase in transfer energy. When X^- lies on the chain axis, d_{z^2} electrons are influenced by a potential barrier coming from the repulsion of X^-, as schematically shown in Fig. 3. The transfer energy T in Eq. (2) is nothing but the tunneling through this barrier. However, under transverse displacement, the barrier decreases and it results in an increased transfer energy. We assume that this increase is proportional to $|q_{\perp l}|$ for the reason given above. T' denotes its proportionality constant.

The last term of Eq. (3) and the function F in it are introduced so as to make the two neighboring X^-'s move in opposite directions, as indicated in Fig. 1. We assume $F(q_{\perp l}q_{\perp,l-1})$ is the following function:

$$F(q_{\perp l}q_{\perp,l-1})=\begin{cases}0 & \text{for } q_{\perp l}q_{\perp,l-1}\le 0 , \\ gq_{\perp l}q_{\perp,l-1} & \text{for } q_{\perp l}q_{\perp,l-1}>0 ,\end{cases} \tag{4}$$

where g is a positive constant of the order of unity.

As one can easily infer, Eq. (3) can produce a uniform increase in the transfer energy. However, we exclude this uniform change because it is already taken into account as a parameter T in $H_{\parallel}$. In order to exclude this effect, we use the $q_{\perp l}$ generated by the following equation:

$$q_{\perp l}=\tilde{q}_{\perp l}-\frac{(-1)^l}{N}\sum_{l'=1}^{N}(-1)^{l'}\tilde{q}_{\perp l'} , \tag{5}$$

where $\tilde{q}_{\perp l}$ is a number that is determined to minimize the total energy, and N is the total number of the sites.

Introducing dimensionless coordinates

$$Q_l[\equiv(\omega/S)^{1/2}q_l],\quad Q_l[\equiv(\omega_{\perp}/S_{\perp})^{1/2}q_{\perp l}] ,$$

we obtain a convenient form for the Hamiltonian, which contains six parameters: T, U, V, S, $S_{\perp}$, and T'. The value of T has been calculated within the Hückel theory by Whangbo and Forshee, and it is about 1 eV.[20] Therefore, using the remaining five parameters U, V, S, $S_{\perp}$, and T', we will systematically investigate the aforementioned eight experiments.

Let us now explain our method to calculate the ground and excited states. In the case of the ground state, we use mean-field theory for interelectronic interactions and the adiabatic approximation for phonons. Within mean-field

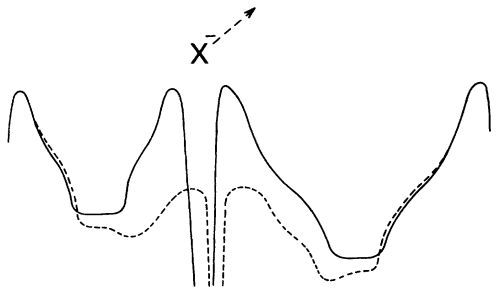

FIG. 3. Schematical pseudopotential for the d_{z^2} electrons as a function of the transverse displacement of X^-. Solid line, without displacement; dashed line, with displacement.

theory, we can approximate H by the mean-field Hamiltonian ($\equiv H_{HF}$), in which $n_{l\sigma}$ and $(a^{\dagger}_{l+1,\sigma}a_{l\sigma})$ are replaced by their averages so that

$$n_{l\sigma}\rightarrow\langle n_{l\sigma}\rangle,\quad (a^{\dagger}_{l+1,\sigma}a_{l\sigma})\rightarrow\langle a^{\dagger}_{l+1,\sigma}a_{l\sigma}\rangle\ .$$

These $\langle n_{l\sigma}\rangle$ and $\langle a^{\dagger}_{l+1,\sigma}a_{l\sigma}\rangle$ are unknown parameters to be determined self-consistently. By diagonalizing this H_{HF}, we can obtain energies of the ground and excited states. In order to take into account the electron-hole correlation in the excited states, we define the difference ($\equiv\Delta H$) between the mean-field Hamiltonian H_{HF} and the true one H as

$$\Delta H=H-H_{HF}\ , \tag{6}$$

and diagonalize it within the basis set of the one-electron excited states obtained from H_{HF}. This is first-order perturbation theory. Then, we can determine the new energies of excited states and their wave functions, including the exciton.

By working this process out for various lattice configurations, we can obtain adiabatic potential-energy surfaces. In numerical calculations, we use a ring that consists of 200 lattice sites occupied by 200 electrons. All the energies are normalized by $T(\approx 1$ eV).

Our way of thinking, in the present paper, is the parameter theory. That is, we will clarify results of the aforementioned eight experiments by using the five adjustable parameters U, V, S, $S_{\perp}$, and T'.

III. RESULTS AND DISCUSSION

First, let us consider the lattice relaxation from the free exciton to the STE. To describe this type of relaxation, we use the following variational function for Q_l, which is the same as that introduced by Mishima and Nasu,[14–16]

$$Q_l=(-1)^l Q\{1+\Delta Q[\tanh\theta(|l|)-1]\}\ , \tag{7}$$

where $(-1)^l Q$ denotes the Peierls distortion in the CDW state, and this Q should be determined beforehand within mean-field theory. The curly brackets $\{\cdots\}$ denote the local lattice displacement from this ground state. ΔQ is its amplitude and θ corresponds to its reciprocal width.

Let us now determine the three parameters U/T, V/T, and S/T. Setting $U/T=1.43$, $V/T=0.79$, and $S/T=0.29$, we can reproduce the three experimental results: the excitation energy of the free-electron-hole pair, the binding energy of the free exciton, and the energy of the luminescence from STE. We shall use these parameters later, and calculate the potential surface, which has not been obtained by experiments to date.

The calculated results and the adiabatic potential-energy surface are shown in Fig. 4, as a function of ΔQ. In this figure, θ is determined to minimize the energy of the first excited state ($\equiv E_{x1}$). All the energies are referenced relative to the ground-state one, and this convention is used hereafter. The transverse displacement does not appear at this stage, because the electron and the hole are not yet sufficiently apart from each other.

The solid line in Fig. 4 is the case of the singlet excitation, and its E_{x1} has the local minimum at around

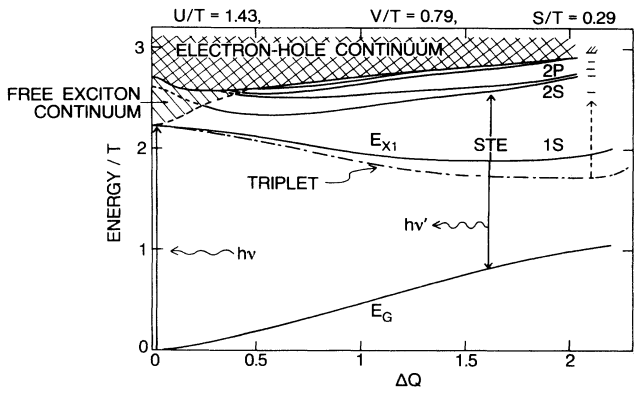

FIG. 4. Adiabatic potential-energy surface from the CT exciton to the STE as a function of ΔQ. θ is determined to minimize E_{x1}. The solid line is singlet, and the dashed line is triplet.

$\Delta Q=1.6$. In this configuration, the calculation shows that $2S$ and the $2P$ states also remain as bound states, as shown in the figure. The charge- and spin-density profiles around the STE are shown in Fig. 5. We can see that a spin-density-wave state has appeared at these five metallic sites. The dashed line in Fig. 4 denotes the triplet exciton. When $\Delta Q=0$, the singlet and the triplet are degenerate, because the exchange interaction becomes zero in our model Hamiltonian H. As ΔQ increases from zero, however, the triplet shifts off from the singlet. It takes the energy minimum at around $\Delta Q=2$, and it is larger than that of the singlet.

As mentioned before, the STE in HMMC is expected to decay into the soliton pair. Next, let us study this channel, using the following variational function for Q_l:

$$Q_l=(-1)^l Q\{1+\Delta Q[\tanh\theta(|l|-l_0/2)-1]\}\ , \tag{8}$$

where θ corresponds to the reciprocal width of a soliton, and l_0 denotes the intersoliton distance. When $l_0=0$, this pattern just corresponds to the STE-type local lattice distortion, Eq. (7). On the other hand, when $l_0\gg 1$ and $\Delta Q=1$, the phase of the Peierls distortion is completely inverted in the region $-l_0/2<l<l_0/2$, which corresponds to the soliton-antisoliton pair.

The adiabatic potential-energy surface calculated using this type Q_l as a function of l_0 is shown in Fig. 6, wherein θ and ΔQ are determined to minimize E_{x1}. Ac-

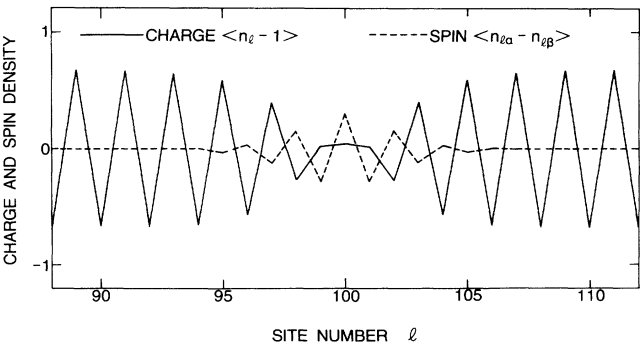

FIG. 5. Charge- and spin-density profiles of the STE.

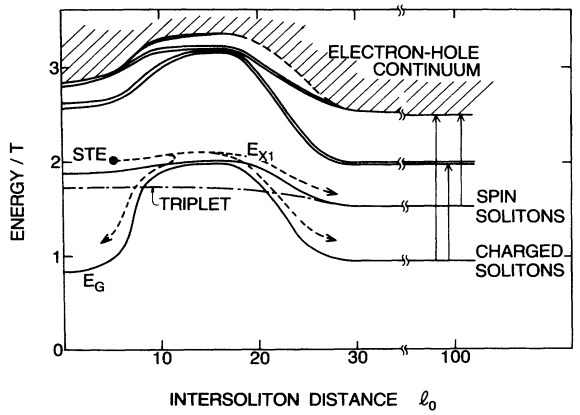

FIG. 6. Adiabatic potential-energy surface from the STE to the solitons as a function of l_0. ΔQ and θ are determined to minimize E_{x1}.

cording to the results of numerical calculations, the first excited state, in the region $l_0 \gg 1$, is a pair of spin solitons, while the ground, second, and third excited states are pairs of charged solitons. The widths of these solitons are about 6 in units of the lattice constant.

As seen from Fig. 6, the singlet STE has three possible relaxation channels. Since the barrier between the STE and the spin-soliton pair is only about 0.1 eV, the singlet STE is expected to decay into spin solitons (lowest excited state) through the tunneling process under the barrier or through the thermal activation process over the barrier. On the other hand, it is also seen that the singlet STE will decay into the charged soliton pair, or return to the CDW ground state. It is a nonradiative process through this barrier region. Because of these three decay channels, the lifetime of the STE is expected to be short. These calculated potential surfaces are qualitatively consistent with the observed lifetime of the STE.[6,7]

From the dashed line in Fig. 6, it can be seen that the triplet STE is unstable, since there is no barrier between the triplet STE and the soliton pair. Incidentally, the energy barrier for the intersite hopping motion of this soliton is about 10 meV.

If a soliton pair is generated, we can expect to get additional light absorption bands due to this soliton, as indicated by the arrows in Fig. 6. The energy of the main absorption band is about one-half of the energy of the CT exciton, and it does not correspond to any of the *A*, *B*, *C*, or *D* bands. We have also taken into account the effects of the transverse displacement on the charged solitons. However, since the positive soliton is not affected by this displacement, the absorption band around the half of the exciton energy remains unchanged. Therefore, it can be concluded that the origin of the photoinduced absorption bands is not solitons.

Next, let us see the relaxation from the STE to a pair of polarons. As for the polaron-type displacements Q_l, we use the following variational function:

$$Q_l=(-1)^l Q\{1+[\Delta Q+\mathrm{sgn}(l)\Delta Q_-]\times[\tanh\theta(||l|-l_0/2|)-l]\}\ , \tag{9}$$

where θ corresponds to the reciprocal width of a polaron, and l_0 denotes the interpolaron distance. $(\Delta Q \pm \Delta Q_-)$ gives the amplitude of the local displacement in the right half ($l>0$) or the left half ($l<0$) of the chain. When $l_0=0$ and $\Delta Q_-=0$, this pattern is just the STE-type local lattice distortion, Eq. (7).

In Fig. 7, we show the adiabatic potential-energy surface as a function of l_0, while θ and ΔQ are determined to minimize E_{x1}. ΔQ_- is fixed to zero, which is the case of two symmetric polarons. In the region $l_0 \gg 1$, the second excited state is a distant pair of polarons, while the first excited state is irrelevant since it returns to the STE when ΔQ_- is introduced. The width of this polaron is 8 in units of the lattice constant.

When such a higher-energy state of the STE as the $2P$ state or the electron-hole continuum is excited, it will relax down to a pair of polarons, since this potential surface has a dissociative nature, as seen from Fig. 7. We can see a very small barrier at around $l_0=20$, which comes from the small overlap between two polarons. Because of this barrier, once the polaron is created, it becomes stable at low temperatures. Incidentally, we have also calculated the potential barrier for a polaron to hop between sites, and it is about 10 meV. Hence the polaron is pinned at low temperatures.

For the case of the hole polaron, the lattice relaxation terminates up to this state. On the other hand, for the electron polaron, it will relax further, because, as we have explained before, an excess electron induces the transverse movements of X^-. Let us consider this effect in connection with the photoinduced absorption.

Figure 8 shows various excitation energies from the electron polaron. In this calculation, the total number of electrons was 201, and $q_{\perp l}$ in Eq. (5) was determined to minimize the total energy. On the left-hand side of this figure, we show the experimental energies of the *A*, *B*, *C*, and *D* bands. The middle of this figure is the theoretical result without $H_\perp$, and corresponds to the case of the hole polaron. We can see that the hole polaron cannot give the *A* and *B* bands, as far as we use the aforementioned values for *U*, *V*, and *S*, which can reproduce the energy of the free-electron-hole pair, the binding energy

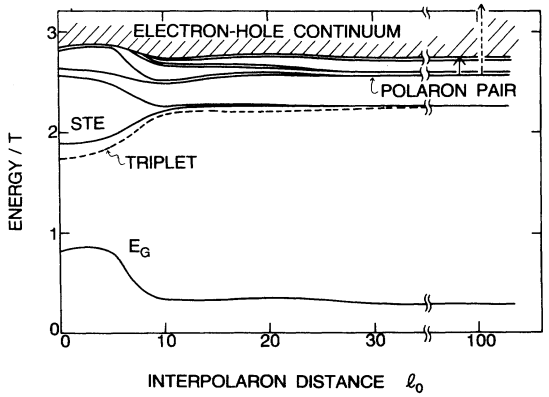

FIG. 7. Adiabatic potential-energy surface from the STE to the polarons as a function of l_0. ΔQ and θ are determined to minimize E_{x1}.

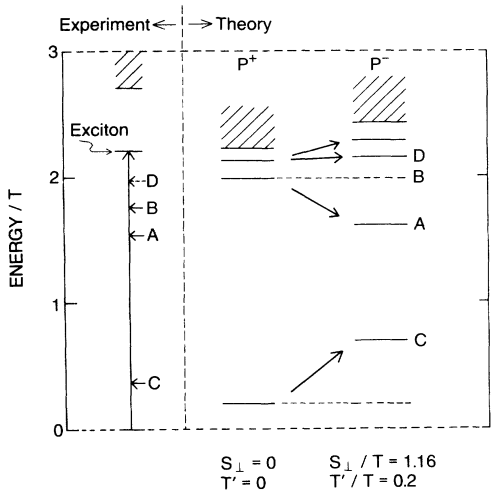

FIG. 8. Excitation energies from the electron polaron.

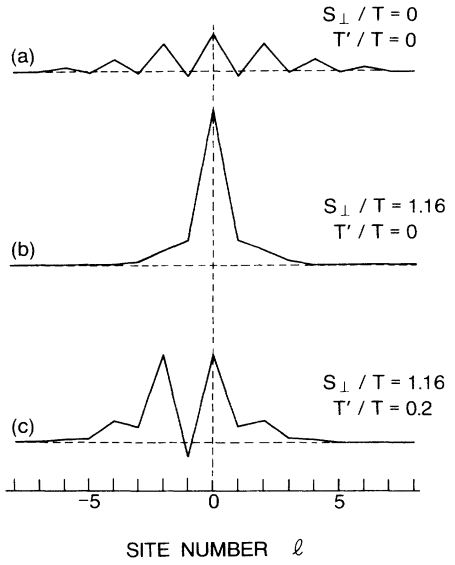

FIG. 9. Spin-density profile of the electron polaron.

of exciton, and the luminescence. On the right-hand side, we show the excitation energies from the electron polaron, fixing $S_\perp/T$ and T'/T at 1.16 and 0.2, respectively. As we mentioned before, $H_\perp$ with these values of $S_\perp$ and T' influences neither the ground state nor the excited states, provided they have no localized excess electron. We can see from this figure that the two excitation energies shift towards the experimental values. The total spectrum is given by the superposition of the electron and hole polaron. Thus we can conclude that the excitation energies calculated here correspond to the *A*, *B*, *C*, and *D* bands.

Figure 9 shows the spin distribution of the electron polaron. Figure 9(a) is the case without $H_\perp$, that is, the case of the hole polaron. The effects of $H_\perp$ are shown in Fig. 9(b) and 9(c). Due to the site-diagonal part of $H_\perp$, the excess electron is trapped more strongly than the hole polaron, as shown in Fig. 9(b). Further, due to the effects of the site-off-diagonal part of $H_\perp$, a bonding state of the excess electron is created between two metals. Consequently, the spin distribution changes from the one-center type to the two-center one, as shown in Fig. 9(c). This strongly localized spin distribution is consistent with the ESR experiment.

Thus, with use of only five adjustable parameters, we have developed a unified picture that can clarify the results of eight rather diverse experiments. That is, the excitation energy of the free-electron-hole pair, the binding energy of the exciton, the luminescence, the four photoinduced absorption bands, and the ESR experiments.

Incidentally, the luminescence from the STE is expected to polarize mainly in the parallel direction. Because of $H_\perp$, however, we can also expect to get a small perpendicular component of luminescence. Wada[21] has already observed such a component, and it is consistent to the present model.

IV. CONCLUSION

We have examined nonlinear lattice-relaxation processes of the exciton in HMMC's, using the extended Peierls-Hubbard model. This model takes into account not only the longitudinal lattice distortion of the X^- but also the component of motion transverse to the chain axis. The effect of strong electron-hole correlation beyond mean-field theory has also been taken into account, and the adiabatic potential-energy surfaces relevant to the relaxation of the exciton have been determined. Eight rather diverse experimental phenomena has been clarified systematically from a unified theoretical point of view. It is concluded that the origin of the photoinduced absorption bands is the electron polaron and the hole polaron.

ACKNOWLEDGMENTS

We wish to acknowledge Dr. Y. Wada for providing the experimental data prior to publication. One of us (M.S.) deeply thanks Professor A. Imamura for his continuous encouragement. The computations were carried out on HITAC M680H and S820 computers at the Institute for Molecular Science. This work is supported by a Grant-in-Aid for Scientific Research on Functionalized Materials (No. 02204005) from Ministry of Education, Science and Culture of Japan.

[1]M. Ueda, H. Kanzaki, K. Kobayashi, Y. Toyozawa, and E. Hanamura, *Excitonic Processes in Solids* (Springer-Verlag, Berlin, 1984); W. Fowler and N. Itoh, *Atomic Processes Induced by Electronic Excitation in Non-Metallic Solids* (World Scientific, Singapore, 1990).

[2]Y. Wada, T. Mitani, M. Yamashita, and T. Koda, J. Phys. Soc. Jpn. **54**, 3143 (1985).

[3]Y. Wada and M. Yamashita, Phys. Rev. B **42**, 7398 (1990).

[4]H. Tanino and K. Kobayashi, J. Phys. Soc. Jpn. **52**, 1446 (1983).

[5]M. Tanaka, S. Kurita, Y. Onodera, T. Kojima, and Y. Yamashita, Chem. Phys. **96**, 348 (1985).

[6]Y. Wada, K. Era, and M. Yamashita, Solid State Commun. **67**, 953 (1988).
[7]H. Tanino, W. Ruhle, and K. Takahashi, Phys. Rev. B **38**, 12716 (1988).
[8]S. Kurita, M. Haruki, and K. Miyagawa, J. Phys. Soc. Jpn. **57**, 1789 (1988).
[9]S. Kurita and M. Haruki, Synth. Metals **29**, F129 (1989).
[10]R. Donohone, S. Ekberg, C. Tait, and B. Swanson, Solid State Commun. **71**, 49 (1989).
[11]N. Matushita, N. Kojima, N. Watanabe, and T. Ban, Solid State Commun. **71**, 253 (1989).
[12]N. Kuroda, M. Sakai, M. Suezawa, Y. Nishina, and K. Sumino, J. Phys. Soc. Jpn. **59**, 3049 (1990).
[13]L. Degiorigi, P. Wachter, M. Haruki, and S. Kurita, Phys. Rev. B **42**, 4341 (1990).
[14]K. Nasu and A. Mishima, Rev. Solid State Sci. **2**, 539 (1988).
[15]A. Mishima and K. Nasu, Phys. Rev. B **39**, 5758 (1989).
[16]A. Mishima and K. Nasu, Phys. Rev. B **39**, 5763 (1989).
[17]A. Bishop and J. Gammel, Synth. Metals **29**, F159 (1989); **29**, F161 (1989).
[18]R. Peierls, *Quantum Theory of Solids* (Oxford University Press, Oxford, 1955), p. 108.
[19]M. Yamashita and K. Toriumi, Inorg. Chim. Acta (to be published).
[20]M. Whangbo and M. Forshee, Inorg. Chem. **20**, 113 (1981).
[21]Y. Wada (private communication).